scientific reports

Check for updates

OPEN

Application of novel nanomaterials with dual functions of antimicrobial and remineralization in mouthwashes

Lin Chang[1,3], Ruihuan Gan[2,3], Xiaoyu Huang[2,3], Dali Zheng[3], Chen Su[3], Youguang Lu[2,3]✉ & Yan Feng[2,3]✉

The study aims to improve the antimicrobial and remineralization-promoting properties of mouthwash by synthesizing novel Ag/ZnO/Oyster Shells nanocomposites and evaluating their anti-caries properties and biosafety in vitro and in vivo, so as to reduce the incidence of caries. The antimicrobial properties of the synthesized Ag/ZnO/Oyster Shell nanocomposites were examined by bacterial inhibition zone, minimum inhibitory concentration, minimum bactericidal concentration, fluorescence staining and scanning electron microscopy. The potential of the materials to promote remineralization of demineralized enamel was detected by scanning electron microscopy, surface microhardness and depth of hard tissue defects, and laser confocal electron microscopy analysis. The synthesized materials were then incorporated into mouthwash, and their effects on antimicrobial properties, remineralization-promoting properties were evaluated. Furthermore, an oral mucosal contact model was established to assess local irritation and systemic effects. The results showed that the novel Ag/ZnO/Oyster Shell nanocomposites possessed strong antimicrobial activity, remineralization-promoting ability and good biosafety, and the mouthwash containing Ag/ZnO/Oyster Shell possessed strong antimicrobial performance and remineralization-promoting ability, and showed no obvious abnormalities in local mucosal tissues, blood indices, and histopathology of the liver and kidneys in the oral exposure model of the SD rats. These findings indicate that Ag/ZnO/Oyster shell incorporated into mouthwash has strong antimicrobial activity, good remineralization-promoting properties and good biosafety in vivo. It is therefore expected to be used in clinical applications.

Keywords Nanocomposites, Mouthwash, Antibacterial, Remineralization properties, Biosafety

According to the recently published Global Burden Disease (GBD), dental caries is the most common disease worldwide, affecting nearly 2.3 billion people[1,2]. The Fourth National Oral Health Epidemiology Survey[3]published in August 2018 showed that the prevalence of caries among Chinese residents was on the rise, with 71.9% in the 5-year-old group, 38.5% in the 12-year-old group, 89.0% in the 35–44-year-old group, and 98.0% in the 65–74-year-old group. The caries process is dynamic, with alternating demineralization and remineralization of tooth structure, and caries can be reversed or arrested even if the loss of minerals in the lesion is sufficient to manifest clinically as a white spot on the tooth surface[4,5]. Therefore, the key to caries control lies in prevention and routine maintenance, including preventing plaque formation, reducing enamel demineralization, and promoting remineralization of lesions[6].

Zinc oxide nanoparticles are potent antimicrobial agents because of their ability to accumulate on bacterial cell membranes by electrostatic attraction. In addition, it has osteogenic, anticancer and remineralization-promoting properties[7–9]. Mouthwashes containing zinc oxide nanoparticles have been shown to have high in vitro activity against cariogenic bacteria[10]and positively impact dentin by impeding its demineralization[11]. Meanwhile, silver nanoparticles have attracted broad attention owing to their low cost, nontoxicity, and high antimicrobial activity[12–15]. According to previous studies, silver nanoparticles were found to not only improve

[1]Department of Rende Road, School and Hospital of Stomatology, Fujian Medical University, Fuzhou, Fujian Province, People's Republic of China. [2]Department of Preventive Dentistry, School and Hospital of Stomatology, Fujian Medical University, Fuzhou, Fujian Province, People's Republic of China. [3]Fujian Key Laboratory of Oral Diseases, School of Stomatology, Fujian Medical University, Fuzhou, Fujian Province, People's Republic of China. ✉email: fjlyg63@fjmu.edu.cn; fengyan@fjmu.edu.cn

the properties of zinc oxide nanoparticles, but also reduce the amount of ingredients[16–19]. In addition, it has also been shown that the combination of antimicrobial materials with calcium compounds (e.g., calcium carbonate, etc.) with remineralization ability is expected to further promote the anti-caries properties of the materials[15,20]. Oyster shells, as a natural green material rich in calcium carbonate and similar to the formation process of natural teeth and bones, have high bioactivity and biocompatibility compared with traditional oral materials, as well as adsorption, biomineralization, and non-toxicity, which can well stabilize and disperse nanoparticles, and can be used as excellent carriers for various antimicrobial agents[11,16,21]. In the previous study, our group synthesized Ag/ZnO/Oyster Shell nanocomposites with good antimicrobial properties by a green method[22,23].

Mouthwash, as a daily-use oral care product, can effectively reduce oral pathogenic microorganisms, and the addition of nano-anti-caries materials to it is a worthy research topic[24,25]. Studies have shown that mouthwashes containing alcohol may cause damage, irritation, or sensitization to oral mucosa or tooth enamel. In this study, a mouthwash with pH above the demineralization threshold of 5.5 and free of fluoride and alcohol was selected as a matrix for nanomaterials to perform the relevant test experiments. In this study, the synthesized Ag/ZnO/Oyster Shell was applied to mouthwash Ora[®] to investigate the antimicrobial and remineralization-promoting properties, which would provide a basis for the subsequent development of a new type of mouthwash with both antimicrobial and remineralization capabilities.

Materials and methods

Antibacterial potential of Ag/ZnO/Oyster Shell

In this study, oyster shell-derived $CaCO_3$was used as a solid support loaded with 2 nm Ag and 10 nm ZnO nanoparticles to construct an efficient Ag/ZnO/Oyster Shell, referring to the relevant literature of previous studies[22,23,26]. The washed and dried oyster shells were powdered in a grinder, sieved through a 200 mesh sieve. 2 g of oyster shells were dispersed in 50 mL of 0.5 mol L^{-1} $Zn(NO_3)_2{\cdot}6H_2O$ solution under magnetic stirring for 24 h. After vacuuming and drying, the ZnO/Oyster Shell nanocomposites were obtained by placing in a muffle furnace and calcined at 600℃ for 4 h with a heating rate of 5℃ min^{-1}. Thereafter, 1 g of the ZnO/Oyster Shell was immersed in 10 mL of 0.1 mol L 1 $AgNO_3$, and 10 mL of *Cacumen platycladi* extract was added. The mixture was combined with magnetic stirring for 48 h without light, and then thoroughly washed with ethanol and water, and dried. For comparison, Ag/Oyster Shell nanocomposites were prepared under similar experimental conditions without the $Zn(NO_3)_2{\cdot}6H_2O$ solution.

The *S. mutans* standard strain (ATCC 25175) and *L. acidophilus* standard strain (ATCC 4356) procured from ATCC were utilized to evaluate the antibacterial potential. *S. mutans* was cultured in BHI broth (Brain Heart infusion broth, Oxoid Ltd, Basingstoke, Hants, UK), and *L. acidophilus* was cultured in MRS broth (de Man, Rogosa and Sharpe Broth, Huankai Microbial, Guangzhou, China). The bacterial suspension was uniformly spread on agar plates, and tablets made of 70 mg of Oyster Shell, Ag/Oyster Shell, ZnO/Oyster Shell or Ag/ZnO/Oyster Shell nanocomposite were each placed on the media for inhibition zone experiment. The agar plates were incubated at 5% carbon dioxide and 37℃ for 24 h and 48 h for *S. mutans* and *L. acidophilus*, respectively. Next, the *S. mutans* and *L. acidophilus* suspension and medium were mixed at a volume ratio of 1 µL:1 mL and dispensed evenly into 6 sterilised centrifuge tubes with a volume of 2 mL per tube. The Ag/ZnO/Oyster Shell suspension was added to each tube with gradient concentrations of 0, 37.5, 75, 150, 300, 600 µg/mL. The *S. mutans* suspension was incubated at 5% carbon dioxide and 37℃ in an orbital shaker for 12 h, while *L. acidophilus* was incubated for 24 h. 100 µL of the medium was transferred to a 96-well plate. The absorbance at 600 nm was measured using a microplate reader (Molecular Devices, USA) to determine the minimum inhibitory concentration (MIC). Each group had 3 auxiliary wells, and each experiment was repeated three times. To determine the production of reactive oxygen species (ROS) in cells, a 20 mM ROS assay kit containing DCFH-DA was used as a fluorescent probe. As a non-fluorescent dye, DCFH-DA is able to penetrate into the cells where it would be hydrolyzed to DCFH. In the presence of intracellular ROS, DCFH is converted into green fluorescent DCF for further analysis. In addition, *S. mutans* and *L. acidophilus* were cultivated in medium with different materials of Ag/Oyster Shell, ZnO/Oyster Shell or Ag/ZnO/Oyster Shell nanocomposite for 6 h and 8 h, respectively. Thereafter, DCFH-DA was added and incubated for 6 h at 37℃. Finally, a fluorescence spectrophotometer (200 Pro, Tecan Infinite, Austria) was used for analysis. Data were normalized by relative expression and statistical analysis by the Student's t test. In addition, FESEM (Tecnai F30, FEI, USA) was used to characterize the microstructure of bacteria under sample treatment. 2 mg of Ag/ZnO/Oyster Shell was added to 10 mL DI water and ultrasonicated for 15 min. Afterward, 1 mL of the sample solution was added to 0.5 mL of the bacterial solution under shaking for 8 h. The bacterial suspension was rinsed three times with PBS, fixed with 35% glutaraldehyde for 30 min, and dehydrated in a graded ethanol series (30, 50, 70, 90, 100%) for 15 min. Finally, bacterial droplets were dried on silicon wafers overnight prior to FESEM observation.

S. mutans was incubated on 24-well plates at 37℃ for 24 h and *L. acidophilus* for 48 h to form mature single-species biofilms, respectively. The original medium in the 24-well plate was replaced and different masses of Ag/ZnO/Oyster Shell composites were added to the new medium to obtain sample suspensions with concentrations of 0, 37.5, 75, 150, 300, 600 and 1200 µg/mL, and incubation was continued for 24 h. Remove the suspended bacteria and medium from the plate, and gently rinse the surface of the biofilm with PBS solution 3 times to remove the floating bacteria and impurities on the surface. Add new corresponding medium, gently blow the adherent bacteria, and elute the bacteria with a turbo-shaker, and take 200 µL into the special microtiter plate, and set up three duplicate wells for each group. Dynamic growth curves of biofilm residual bacteria after sample treatment were recorded and plotted using a Bioscreen automated growth curve analyzer (Bioscreen C Pro, Finlan Inc.), which measured optical density (OD) at a wavelength of 600 nm under constant medium-rate oscillations at 37℃ for a period of 48 h. Furthermore, the live/dead assay was performed using a 200 µL live/dead kit (Thermo Fisher, USA) to soak the treated biofilm residual bacteria in another sample plate for 30 min under a fluorescence microscope (Zeiss, Germany). The excitation and emission wavelengths of SYTO9 are 480

and 500 nm respectively, and those of PI are 490 and 635 nm respectively. Each group had 3 auxiliary wells, and each experiment was repeated three times.

Biosafety Research of Ag/ZnO/Oyster Shell

This study was conducted to the ethical guideline of Declaration of Helsinki and was approved by the institutional ethics committee of School and Hospital of Stomatology, Fujian Medical University. After obtaining informed consent from the patients, gingival tissues were cut from the margins of the third molar extractions, and human gingival fibroblasts (HGFs) cells were separated and cultured. Cell samples were sent for Short Tandem Repeats (STR) identification. The medium was low-sugar Dulbecco's modified eagle medium (DMEM), 10% Fetal Bovine Serum (FBS), and 1% antibiotic. 15 mg of Ag/ZnO/$CaCO_3$ nanocomposite was weighed and added to 45 mL of low sugar DMEM culture solution. The supernatant was collected by centrifugation at 8000 rpm for 5 min, and then 5 mL of 10% FBS and 1% antibiotic mixture was added to form a final concentration of 300 μg/mL of sample extract culture medium, and then the culture medium was diluted twice to obtain 75 and 150 μg/mL of sample extract culture medium. The blank group was cell culture medium containing different concentrations of sample extracts. The cells were then inoculated in 96-well plates for 72 h. The original medium was discarded and washed twice with PBS solution. 110 μL of culture medium containing 10 μL of Cell Counting Kit-8 (CCK-8) was added to each well and the plates were incubated at 37 °C for 1 h. The OD was measured at 450 nm.

$RGR = \frac{ODn - ODblank}{ODcontrol - ODblank}$. Each group had 3 auxiliary wells, and each experiment was repeated three times. Three random microscopic photographs were taken in each group.

Remineralization Research of Ag/ZnO/Oyster Shell

This study was approved by the institutional ethics committee of School and Hospital of Stomatology, Fujian Medical University. Freshly extracted orthodontic premolar teeth were collected and cut into enamel blocks using a low-speed precision cutter (IsoMet1000, Buehler Corporation, USA). The surface was polished under running water with 800, 1500, 2000 and 2400 grit sandpaper. A 3 × 3-mm window was left in the center of the surface and surrounded by acid-resistant nail polish[27]. To establish a demineralization model, the samples were placed in the demineralization solution (2.2 mM $Ca(NO_3)_2$, 2.2 mM KH_2PO_4, 50 mM CH_3COOH, 1.0 mM NaN_3, 0.1 mM NaF, pH adjusted to 4.5) under magnetic stirring at 50 rpm for 72 h. The demineralization solution was replaced every 24 h. The samples were randomly grouped according to the hardness value of the samples after demineralization, with 15 samples in each group. The pH cycling was carried out with experimental group of 300 μg/mL Ag/$CaCO_3$, 300 μg/mL ZnO/$CaCO_3$, 300 μg/mL Ag/ZnO/$CaCO_3$, the negative ddH_2O and the positive NaF control group[28], under magnetic stirring at 37 °C and 50 rpm, including 2 h demineralization and 22 h remineralization (20 mM HEPES, 0.9 mM KH_2PO_4, 1.5 mM $CaCl_2$, 130 mM KCl, 1.0 mM NaN_3, pH adjusted to 7.0.). The treatment was carried out before and after demineralization. The sample was placed into the treatment solution under magnetic stirring at 37 °C at 50 rpm for 3 min each time. The entire pH cycling lasted for 12 d[29–31].

Vickers hardness was measured by a microhardness tester (HXD-1000TM/LCD, Taiming, China) under 50-gf load for 10 s. Three points (100 μm apart) were randomly measured in the windowed area of each sample, and each point was measured three times. The average value was taken as the baseline SMH_0, SMH_1 after demineralization, and SMH_2 after pH cycling. The surface profilometer (SEF680, Kosaka Institute, Japan) randomly selects the window area and enamel surface. The height difference between datum plane and treatment surface was regarded as the depth of the surface hard tissue loss[32]. The sampling length was 0.8 mm, the measuring length was 2.0 mm, and the testing speed was 0.5 mm/s. The average Ra value is regarded as the surface roughness. In addition, 6 samples were randomly selected from each group and the surface and cross-sectional images after sputtering gold were observed by field emission scanning electron microscopy (FESEM)[33]. Furthermore, after stained with 0.1 mmol/L rhodamine B for 1 h in the dark, the samples were examined by confocal laser scanning microscopy (CLSM) using a Carl Zeiss SP8 laser confocal microscope, and the scanning plane should be 50 μm below the surface to avoid the interference of the smear layer[34].

IBM SPSS 25.0 statistical analysis software was applied, and all the data were checked for normal distribution using the Kolmogorov-Smirnov test. The data were analysed by One-way analyses of variance (ANOVA), and a P-value < 0.05 was measured as statistically significant.

Preparation and Property of Mouthwash containing Ag/ZnO/Oyster Shell

Among the various mouthwashes available on the market, the fluorine-free and alcohol-free Ora® Bright White Mouthwash was chosen as an ingredient because of its pH value > 5.5. 150 mg of Ag/ZnO/Oyster Shell was weighed and added into 500 mL of mouthwash, ultrasonicated for 10 min, and then left at room temperature for 24 h. The supernatant was collected by centrifugation at 8000 rpm for 15 min, and then the mouthwash was configured into a final concentration of 300 μg/mL of Ag/ZnO/Oyster Shell Ora® mouthwash. Moreover, relevant antimicrobial, biosafety research and remineralization properties of mouthwash was detected as described above according to the standards of ISO 16408 – 2015.

Animal Research of New Mouthwash

Mouthwash to mucosa irritation experiment reference standard (YY/T 0127.13, China[35]) were approved by the Animal Care and Use Committee of Fujian Medical University (approval number FYKQ-2018-036). And all experiments were performed in accordance with relevant guidelines (ARRIVE guidelines 2.0) and regulations methods. Twelve male specific-pathogen-free (SPF) SD rats (7–8 weeks old) with healthy mucosa were obtained from Shanghai Jihui Experimental Animal Breeding Company, China. The SD rats were randomly and evenly divided into three groups. Random numbers were generated using the standard = RAND() function in

Microsoft Excel. Rats were anesthetized with isopropaner by inhalation, and the perioral area was disinfected with iodophor. Bilateral buccal and tongue mucosa of rats were coated with 5 mL of mouthwash, mouthwash containing Ag/ZnO/Oyster Shell, or ddH_2O respectively, for 3 min each. The operation totaled 14 days, twice a day.

8 mL of blood was taken from each rat, placed in a water bath at 37 °C for 15 min and centrifuged at 3000 r/min for 5 min to obtain at least 2 mL of serum. Hepatocyte damage index in serum, such as aspartate transaminase (AST) and alanine transaminase (ALT), and renal function indexes: serum urea nitrogen (BUN) and serum creatinine (CREA) were detected using an automatic biochemical analyzer.

The buccal mucosa tissue about 2 × 1 × 0.5-cm and the lingual mucosa tissue about 4 cm× 1 cm× 0.5-cm were collected respectively, fixed in 4% paraformaldehyde for 24 h. The tissues were then stained with hematoxylin-eosin (HE) and the mucosal tissues were evaluated microscopically by two histopathologists according to YY/T 0127.13. At the end of the experiment, the rats were euthanised with 2% Sodium pentobarbital (100 mg/kg).

Results

Ag/ZnO/Oyster Shell nanomaterials have the ability to inhibit the plaque of cariogenic bacteria

Compared with Oyster Shell (0.50 cm), ZnO/Oyster Shell (0.50 cm) and Ag/Oyster Shell (0.72 cm), Ag/ZnO/Oyster Shell (0.80 cm) showed a larger zone of inhibition against *S. mutans* (Fig. 1A). Similarly, Ag/ZnO/Oyster Shell (0.78 cm) compared to Oyster Shell (0.50 cm), ZnO/Oyster Shell (0.55 cm) and Ag/Oyster Shell (0.72 cm) showed a larger zone of inhibition against *L. acidophilus* (Fig. 1B), suggesting stronger antibacterial activity. As shown in Fig. 1C and E, the Ag/ZnO/Oyster Shell at concentrations of 75 μg/mL and 150 μg/mL can completely inhibit the growth of *S. mutans* and *L. acidophilus*, while the colony-forming units of bacteria were reduced to zero at a concentration of 300 μg/mL and 600 μg/mL, respectively. As compared to the binary Ag/Oyster Shell and ZnO/Oyster Shell, Ag/ZnO/Oyster Shell produced an approximate 2-fold increase of ROS. All of these studies revealed that the Ag/ZnO/Oyster Shell were capable of producing ROS, and resulted in irreversible DNA damage and bacteria death (Fig. D). Additionally, SEM observations (Fig. 1F and G) showed that untreated *S. mutans* were smooth spherical or ovoid in shape. When co-cultured with the samples, the cell membrane was damaged and distortion, resulting in the leakage of intracellular components and finally cell lysis. Similarly, *L. acidophilus* was initially elongated with rounded ends, whereas after Ag/ZnO/Oyster Shell treatment, the surface became rough, the organism to shrank into short rods, with cell contents leaking and blurring the surface morphology of the nanomaterials (Fig. 1H and I). These results suggest that Ag/ZnO/Oyster Shell disrupted the structure of the bacteria, causing it to deform or disintegrate, which in turn led to the death of the bacterial cell.

The common cariogenic bacterium *S. mutans* or *L. acidophilus* usually exists in the form of plaque biofilm. The inhibitory effect of Ag/ZnO/Oyster Shell on the formed biofilms of *S. mutans* or *L. acidophilus* was further investigated through a series of experiments. As shown in Fig. 2A and B, the residual bacteria in *S. mutans* and *L. acidophilus* biofilm began to be inhibited when the material concentrations reached 150 μg/mL and 300 μg/mL, respectively. Moreover, under the microscope, *S. mutans* and *L. acidophilus* biofilm in the control groups displayed a large amount of green fluorescence and a small amount of red fluorescence, while the Ag/ZnO/Oyster Shell groups exhibited the opposite (Fig. 2C and D).

Ag/ZnO/Oyster Shell Nanomaterials have good biosafety

Ag/ZnO/Oyster Shell nanomaterials were added to HGF cells and the viability of the cells was assayed for cytotoxicity using the cck-8 assay. The results in Fig. 3A showed that the material at a concentration of 75 μg/mL did not have a significant effect on cell proliferation compared to the negative control. Figure 3B showed the relative proliferation rates of HGFs, which were $(97.55 \pm 1.36)\%$, $(80.92 \pm 1.62)\%$ and $(62.27 \pm 1.52)\%$, respectively, where the cytotoxicity of the 75 and 150 μg/mL groups was non-cytotoxic, and the cytotoxicity of the 300 μg/mL group was slightly cytotoxic, and none of them were recognized as having cytotoxicity. The microscopic structural morphology of HGFs was shown in Fig. 3C, and the growth was consistent with CCK-8 and RGR results.

Ag/ZnO/Oyster Shell promotes remineralization

The pH cycle model (Fig. 4A) can mimic the caries process well and is therefore widely used to estimate the anti-caries potential and to promote remineralization properties[36]. The results in Fig. 4B and C showed an increase in hardness recovery and a decrease in surface hard tissue loss after treatment with Ag/ZnO/Oyster Shell and positive control NaF as compared to the negative control ddH_2O. In contrast, no significant difference was observed in hardness recovery and the depth of surface hard tissue loss in the binary composite Ag/Oyster Shell and ZnO/Oyster Shell compared to the negative control. The results of the CLSM research (Fig. 4D and E) were consistent with the abovementioned results.The results showed significantly lower fluorescence area and average fluorescence for both Ag/ZnO/Oyster shells and the positive control compared to the negative control, suggesting a smaller amount of mineral loss. Whereas no significant differences were seen in all three aspects between the negative control, the binary material Ag/Oyster Shell and ZnO/Oyster Shell.

Mouthwash containing Ag/ZnO/Oyster Shell possessed strong properties

The mouthwash containing Ag/ZnO/Oyster shells was a pale yellow, clarified and unadulterated solution with a pH of 6.6. As shown in Fig. 5A, the novel mouthwash is capable of achieving a good bacteriostatic effect as the existing mouthwash due to the surfactant and foaming agent components. Compared with the negative control ddH_2O, the hardness recovery and the hard tissue loss (Fig. 5B and C) treated by new mouthwash and the mouthwash containing NaF changed significantly ($P < 0.05$). SEM observation of enamel cross-sectional morphology, as seen in Fig. 5D-G, the control-treated enamel column was rough, and the center was dissolved

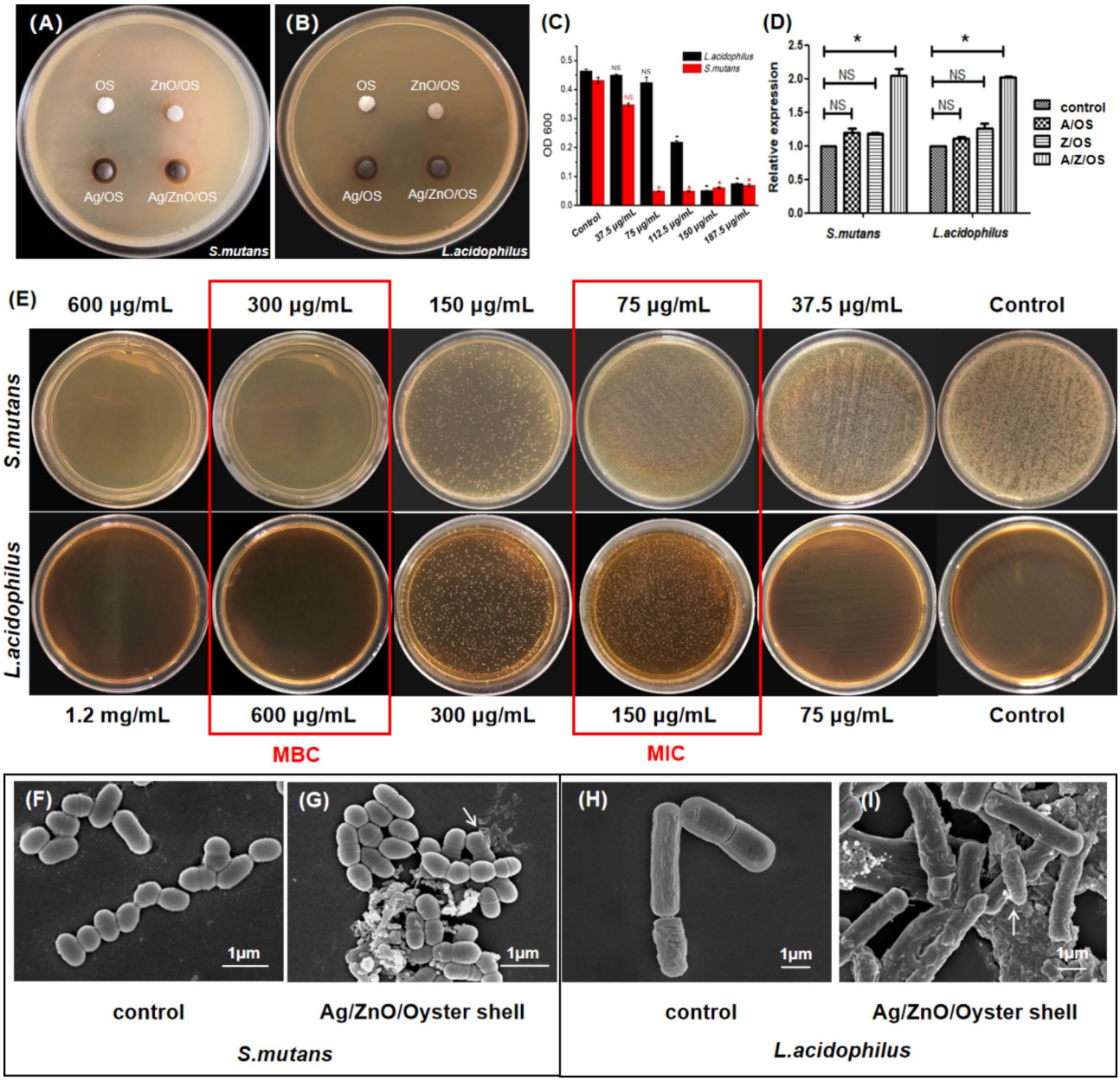

Fig. 1. Inhibition effects of Ag/ZnO/Oyster Shell on *S. mutans* and *L. acidophilus*. The inhibition zone of agar plates of *S. mutans* (A) and *L. acidophilus* (B) treated with Ag/ZnO/Oyster Shell. The absorbance histograms and agar plates of *S. mutans* and *L. acidophilus* suspension (C and D). SEM images of *S. mutans* (E and F) and *L. acidophilus* (G and H).(*:$P < 0.05$).

and destroyed, while the morphology of the enamel columns treated with mouthwash, new mouthwash, and NaF containing mouthwash did not show any obvious damage. Besides scattered mineral deposition particles were seen on the surface of the enamel columns treated with new mouthwash. As shown in Fig. 5H, the fluorescence excited in the lesion areas of the control-treated and mouthwash-treated groups was higher than that of the other two groups in terms of area and intensity, indicating a greater loss of minerals. Whereas no significant differences were seen between the new mouthwash group and the NaF-containing group.

After 14 days of the mucosal experiment (Fig. 6A), comparing the control, new mouthwash and mouthwash groups, there was no significant difference in the liver function indexes ALT and AST and kidney function indexes BUN and CREA in each group of rats, as shown in Fig. 6B. Figure 6C showed the pathomorphology of the buccal and lingual mucosa of the rats after the experiment, none of which were significantly different. After the pathologist's reading and scoring, the score of buccal mucosa was 0.07 and the lingual mucosa score was 0 in all three groups, suggesting that there was no mucosal irritation in all three groups.

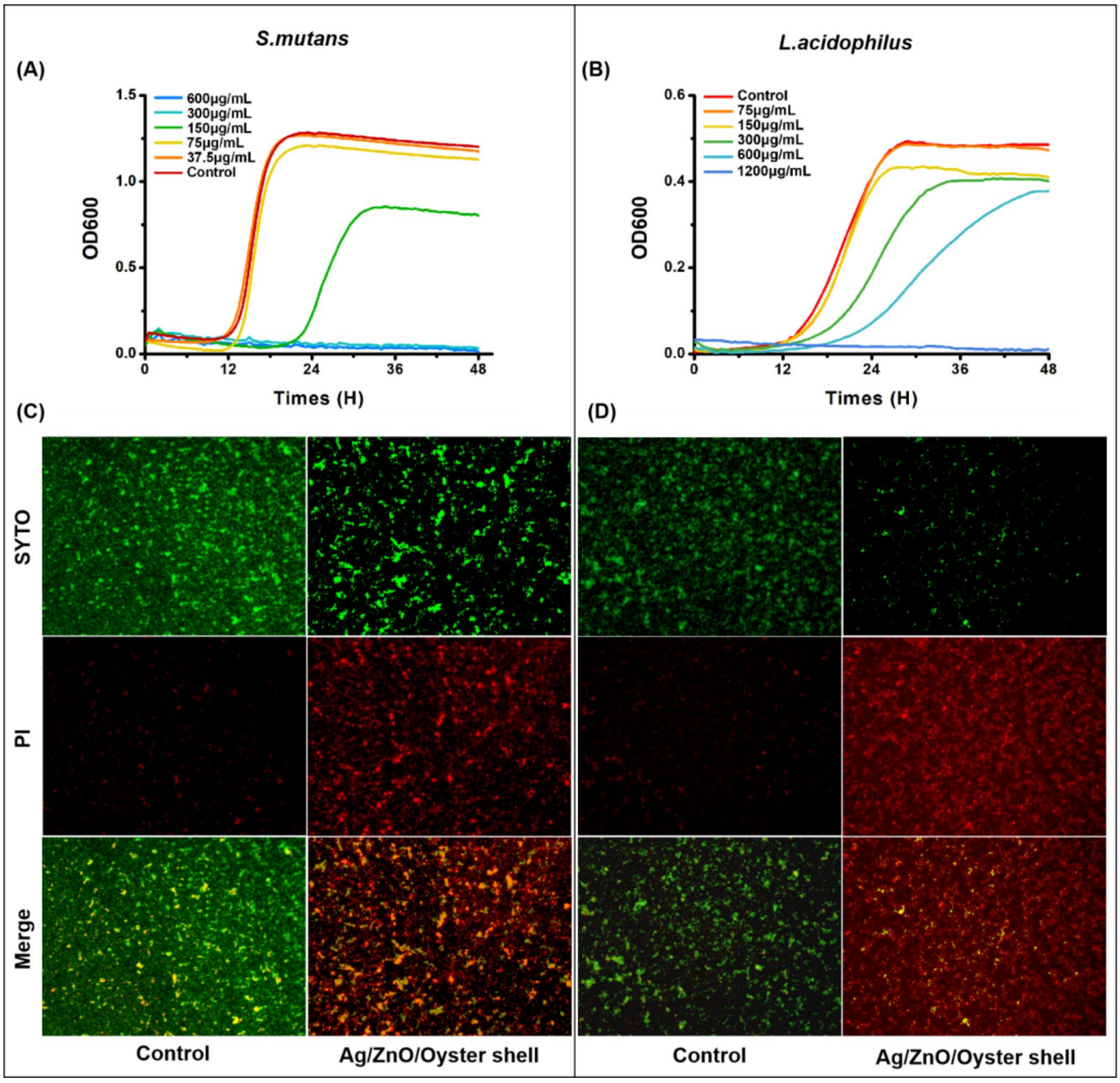

Fig. 2. Inhibition effects of Ag/ZnO/Oyster Shell on *S. mutans* and *L. acidophilus* biofilm. The growth curve of residual *S. mutans* biofilm (A) and *L. acidophilus* biofilm (B). Fluorescence staining (SYTO9/PI, ×100) of *S. mutans* biofilm (C, 150 μg/mL) and *L. acidophilus* biofilm (D, 600 μg/mL).

Discussion

The inhibitory effect of Ag/ZnO/Oyster Shell nanocomposites on bacteria may be related to the synergistic antimicrobial properties of silver nanoparticles and zinc oxide nanoparticles. Studies on the antibacterial mechanism have shown that silver nanoparticles and zinc oxide nanoparticles can establish contact with bacteria. Contacts can be made through van der Waals forces[37], electrostatic interactions[38], hydrophobic interactions[39], and receptor ligands[40]. Subsequently, nanoparticles act on the cell membranes by releasing metal ions[41]or enter the bacteria to cause oxidative stress[42], which alters cell membrane permeability, disrupting the electrolyte balance, inhibiting and inactivating certain enzymes, generating oxygen-active free radicals, disrupting cellular metabolic processes, and ultimately leading to microbial death. It may also inhibit bacterial DNA replication, affect ATP production and alter gene expression[43,44]. The antimicrobial activity of silver nanoparticles is influenced by the concentration of silver ions they release. It is also affected by its particle size, and its biological activity and stability increase with decreasing particle size[45,46]. Smaller silver nanoparticles have a higher surface area-to-volume ratio, which allows them to penetrate biological surfaces more readily, disrupting the lipid bilayer by interacting with cell membranes, leading to an increase in membrane permeability and thus bacterial lysis[47,48]. It has been shown that silver nanoparticles with particle size between 5 and 20 nm have stronger

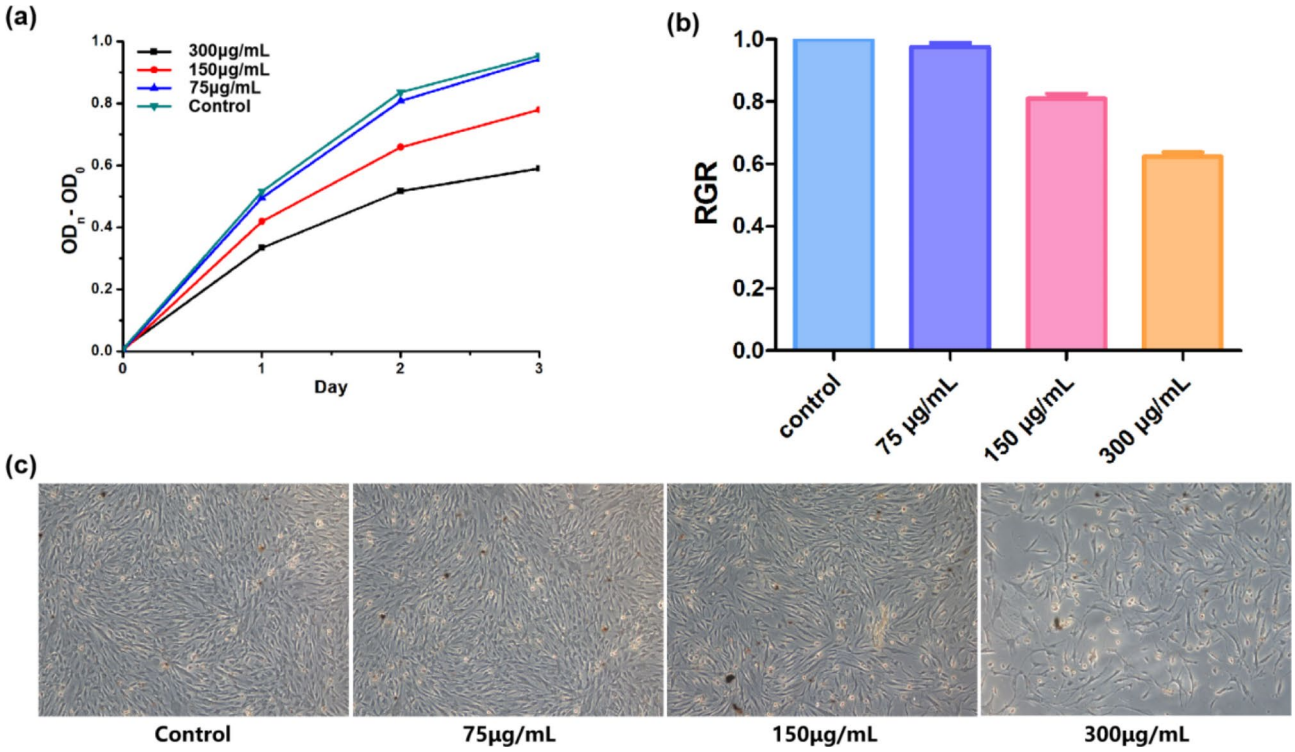

Fig. 3. Effect of Ag/ZnO/Oyster Shell against HGFs. Plot of changes of OD450 (A). Relative growth rate (RGR) of HGFs (B). (C) Morphology of HGFs (×100).

antibacterial activity against Staphylococcus aureus compared to those with particle size of 30 nm[49]. In the Ag/ZnO/Oyster Shell synthesized in this study, the silver nanoparticles have a particle size size of about 2–10 nm, which is structurally superior. On the other hand, studies on the antimicrobial mechanism of ZnO nanoparticles have shown that ZnO nanoparticles can generate a large amount of ROS, such as OH^-, H_2O_2, and O^{2-}, which cause oxidative stress in bacteria and lead to cell death[50]. The incorporation of silver nanoparticles better serves as an electron reservoir, which enhances the production of ROS[51].

Furthermore, it has been shown that more than 60% of microbial infections are associated with biofilm formation[52]. Since biofilms are stable colonies that protect bacteria from environmental challenges, inhibiting biofilms is inherently more challenging than killing planktonic bacteria[53]. In this study, we explored the inhibitory effect of single bacterial biofilms of Streptococcus mutans and Lactobacillus acidophilus, which often exist in the form of biofilm, by using Ag/ZnO/Oyster Shell treatments containing different concentrations of Ag/ZnO/Oyster Shell after culturing Streptococcus mutans and Lactobacillus acidophilus to form a biofilm, and carried out residual bacterial kinetic tests and SYTO9/PI staining experiments in a targeted manner. The results showed that when the concentration of Ag/ZnO/Oyster Shell was greater than 300 μg/mL, it could almost completely inhibit the growth of the residual bacteria in the biofilm of Streptococcus mutans and lead to the death of more than half of Lactobacillus acidophilus biofilm bacteria, and the bactericidal effect was more obvious with the increase of the concentration.

Regarding the study on the remineralization capacity of enamel, Ag/ZnO/Oyster Shell showed a clear pro-remineralization effect. During enamel demineralization, hydroxyapatite crystals dissociate and diffuse by acid, resulting in the loss of calcium and inorganic salts such as Ca^{2+}, CO_3^{2-} and OH^-. Oyster shells are primarily composed of calcium carbonate ($CaCO_3$, 80–85%) and also contain calcium phosphate ($Ca_3(PO_4)_2$), and calcium sulfate($CaSO_4$)[54]. In the oral salivary environment, Ca^{2+}, HCO_3^-, CO_3^{2-}, OH^-, and PO_4^{3-} increase the local ion concentrations, thereby reversing enamel demineralization. At the same time, Ca^{2+}, CO_3^{2-}, OH^-also neutralize external acids and reduce enamel demineralization damage. In addition, some studies in vitro have shown that zinc is not only an important component of enamel, and its distribution and amount in enamel may affect caries progression, but zinc ions are also known to reduce the rate of enamel demineralization[55,56]. It has been reported that hydroxyapatite pretreated with zinc ions has the ability to resist acid dissolution at a level similar in magnitude to that of fluorine at equivalent molar concentrations[57]. In this study, the results of ZnO/$CaCO_3$-treated group did not show any significant difference compared to the negative control, whereas the Ag/ZnO/Oyster Shell group showed a significant pro-remineralization effect, which may be attributed to the increase in the efficacy of ZnO nanoparticles caused by the addition of silver nanoparticles. Compared to raw material mouthwash, the results of the study suggest that Ag/ZnO/Oyster Shell-containing mouthwash has a certain effect of promoting enamel remineralization.

In this study, the biosafety of this material was further explored by in vivo animal experiments with reference to the YY/T 0127.13–2018 standard. By simulating the use of mouthwash, which was applied to the oral mucosa

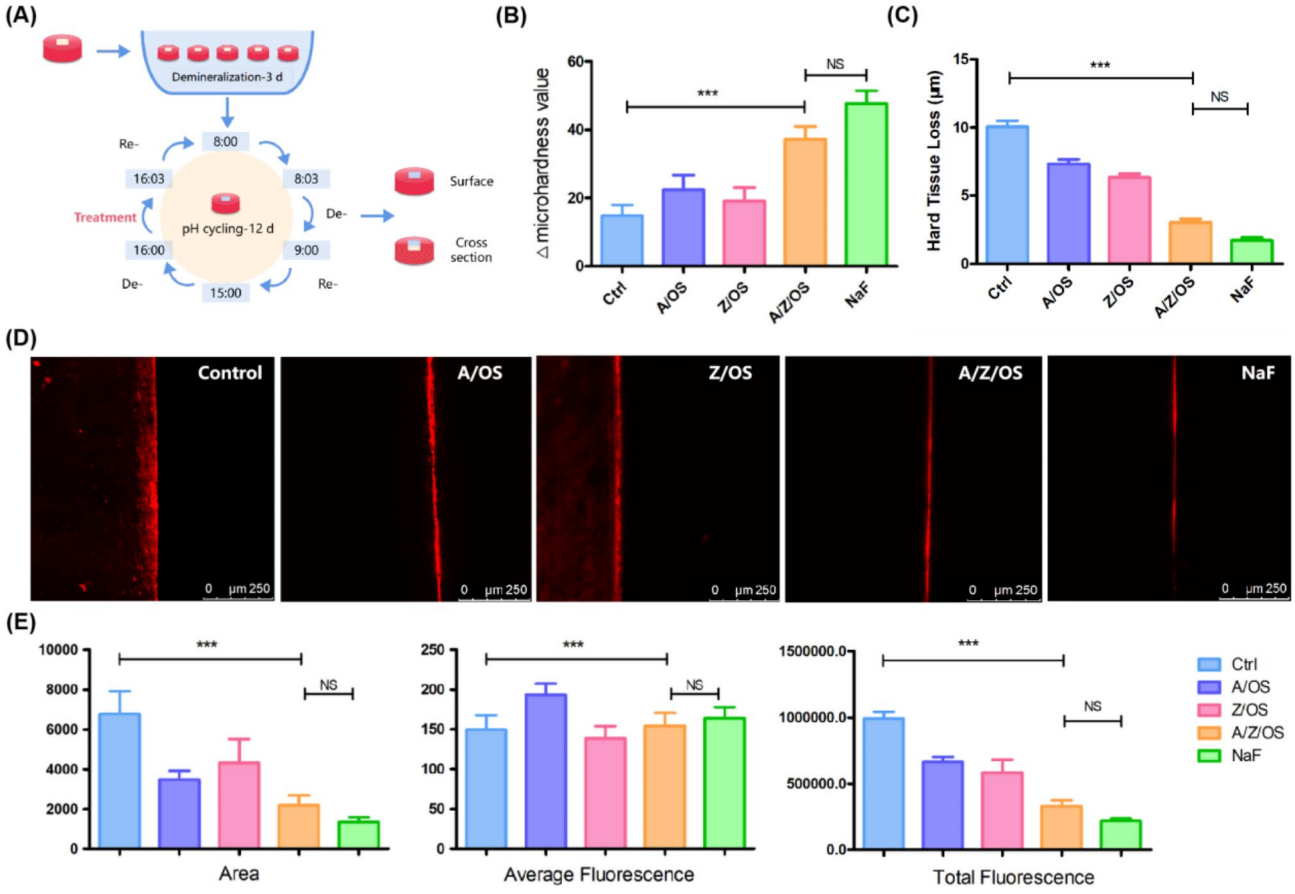

Fig. 4. Remineralization effect of Ag/ZnO/Oyster Shell. Scheme for the pH cycling of enamel(A). Changes in surface microhardness values (B). Changes of hard tissue loss (C). Images (D) and variations (E) in the result of CLSM (***:$p < 0.05$).

of rats twice a day, the pathological morphology of the buccal and lingual mucosal tissues of rats was compared among the use of the negative control ddH_2O, the Ag/ZnO/Oyster Shell-containing mouthwash, and the mouthwash, and was scored by a pathologist who examined the slides under a microscope, and the results showed that there was no mucosal irritation in any of the three groups. In addition, in this study, the serum liver function indexes ALT and AST and kidney function indexes BUN and CREA of rats treated with different treatments were checked, and the results did not show any remarkable abnormality. This indicates that the new mouthwash has no significant effect on the liver and kidney functions of rats and has good biological safety.

Conclusion

Mouthwash containing Ag/ZnO/Oyster Shell exhibited a strong inhibitory effect on common carious bacterial biofilms and has a high potential in enamel remineralization. Additionally, its lack of irritation to mucosal tissues and its favorable safety profile in vivo experiments suggest a wide range of clinical applications.

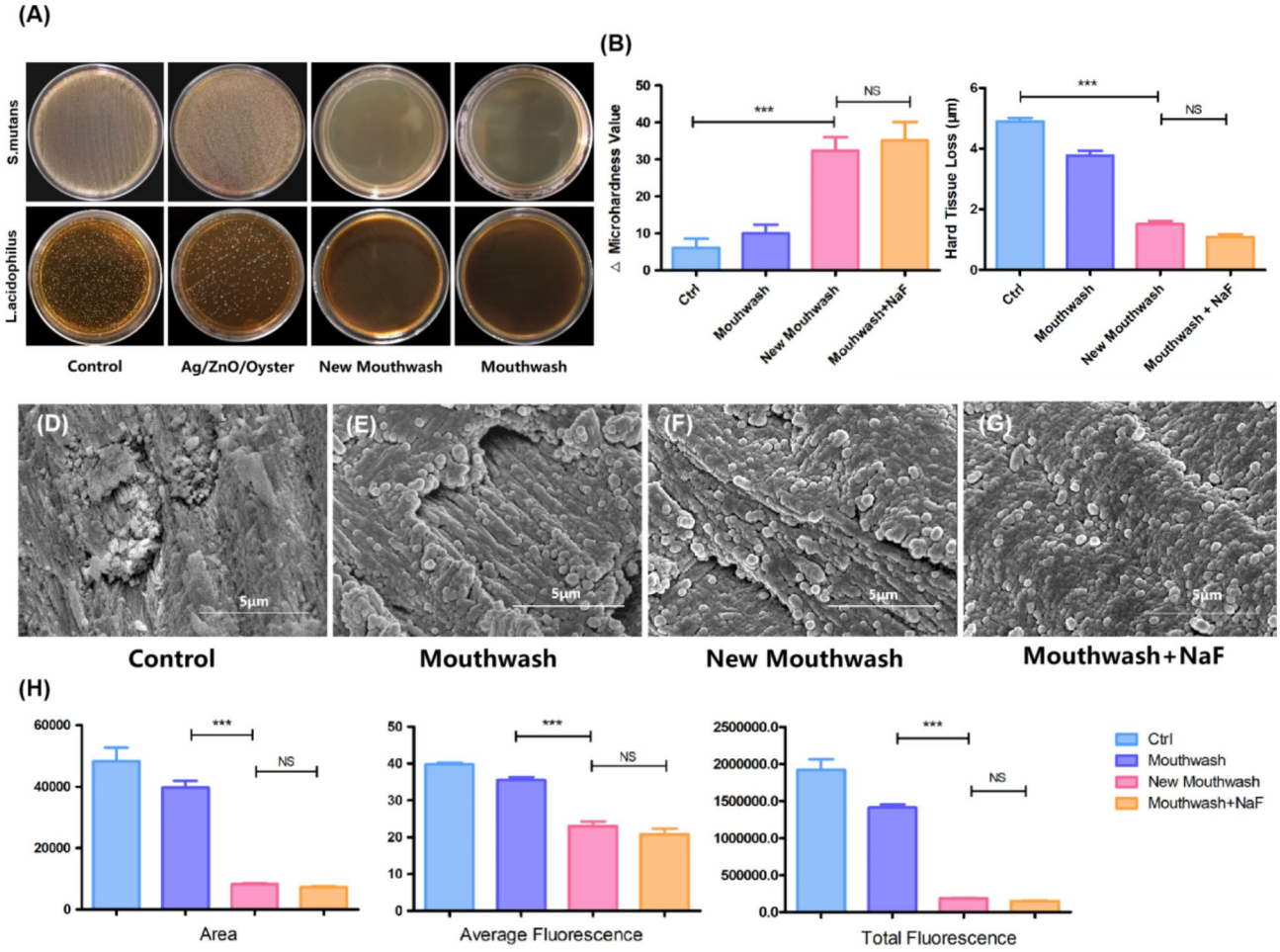

Fig. 5. Inhibition and remineralization effect of mouthwash containing Ag/ZnO/Oyster Shell. Agar plates of *S. mutans* and *L. acidophilus* biofilm treated with different materials (A). Changes in surface microhardness values (B) and hard tissue loss (C). SEM images of enamel (D-G). Changes (H) in the result of CLSM treated with different materials (***:$p < 0.05$).

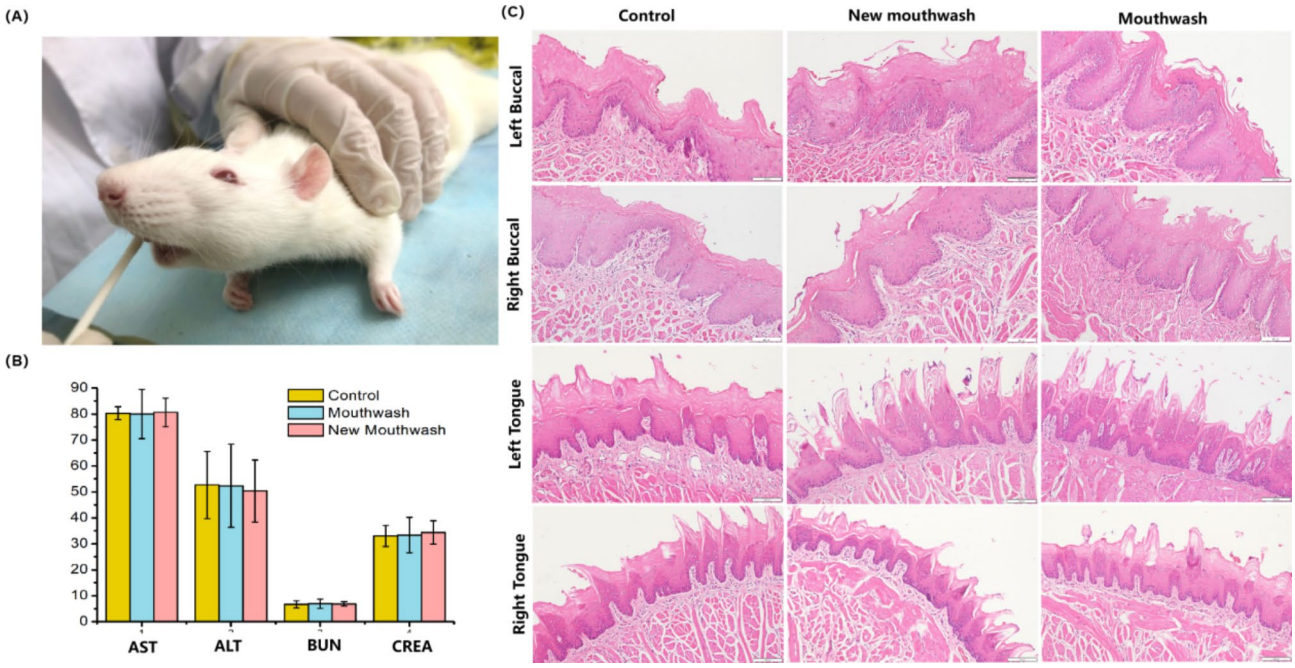

Fig. 6. Mucosal contact test of SD rats. (A) Smear mouthwash on buccal and lingual mucosa. (B) Liver and kidney function index. (C) HE staining of buccal and lingual mucosa (×400).

Data availability

Data is provided within the manuscript or supplementary information files.

Received: 3 July 2024; Accepted: 21 November 2024
Published online: 23 November 2024

References

1. Peres, M. A. et al. Oral diseases: a global public health challenge. *Lancet* **394**, 249–260 (2019).
2. Bernabe, E. et al. Global, regional, and national levels and trends in burden of oral conditions from 1990 to 2017: a systematic analysis for the global burden of disease 2017 study. *J. Dent. Res.* **99**, 362–373 (2020).
3. Wang Xing. *The Fourth National Oral Health Epidemiological Survey Report*p. 50 (People's Medical Publishing House, 2018). 77,103,104.(Chinese).
4. Sundararaj, D., Venkatachalapathy, S., Tandon, A. & Pereira, A. Critical evaluation of incidence and prevalence of white spot lesions during fixed orthodontic appliance treatment: a meta-analysis. *J. Int. Soc. Prev. Community Dentistry*. **5** (6), 433–439 (2015).
5. Khoroushi, M. & Kachuie, M. Prevention and Treatment of White Spot lesions in Orthodontic patients. *Contemp. Clin. Dent.* **8** (1), 11–19 (2017).
6. Edelstein, B. L. The dental caries pandemic and disparities problem. *BMC Oral Health*. **6** (Suppl 1), S2 (2006).
7. Yu, H., Chen, G., Wang, Y. & Yao, J. A facile one-pot route for preparing cellulose nanocrystal/zinc oxide nanohybrids with high antibacterial and photocatalytic activity. *Cellulose* **22** (1), 261–273 (2014).
8. Sondi, I. & Salopek-Sondi, B. Silver nanoparticles as antimicrobial agent: a case study on E. Coli as a model for Gram-negative bacteria. *J. Colloid Interface Sci.* **275** (1), 177–182 (2004).
9. Grenho, L., Salgado, C. L., Fernandes, M. H., Monteiro, F. J. & Ferraz, M. P. Antibacterial activity and biocompatibility of three-dimensional nanostructured porous granules of hydroxyapatite and zinc oxide nanoparticles–an in vitro and in vivo study. *Nanotechnology* **26** (31), 315101 (2015).
10. Kachoei, M. D., Baharak;Tabriz, F. & Dabaghi A comparative study of antibacterial effects of mouthwashes containing Ag/ZnO or ZnO nanoparticles with chlorhexidine and investigation of their cytotoxicity. *Nanomed. J.* **5** (2), 102–110 (2018).
11. Takatsuka, T., Tanaka, K. & Iijima, Y. Inhibition of dentine demineralization by zinc oxide: in vitro and in situ studies. *Dent. Mater.* **21** (12), 1170–1177 (2005).
12. Dias, H. B. et al. Synthesis, characterization and application of Ag doped ZnO nanoparticles in a composite resin. *Mater. Sci. Engineering: C.* **96**, 391–401 (2019).
13. Salaie, R. N., Besinis, A., Le, H., Tredwin, C. & Handy, R. D. The biocompatibility of silver and nanohydroxyapatite coatings on titanium dental implants with human primary osteoblast cells. *Mater. Sci. Engineering: C.* **107**, 110210 (2020).
14. De Matteis, V. et al. Silver nanoparticles addition in poly(Methyl Methacrylate) Dental Matrix: Topographic and Antimycotic studies. *Int. J. Mol. Sci.* **20** (19), 4691 (2019).
15. Porter, G. C. et al. Anti-biofilm activity of silver nanoparticle-containing glass ionomer cements. *Dent. Mater.* **36** (8), 1096–1107 (2020).
16. Jing, X. et al. Preparation of Ag/α-Al2O3 for ethylene epoxidation by an impregnation-bioreduction process with Cinnamomum camphora extract. *Chem. Eng. J.* **284**, 149–157 (2016).
17. Sinha, T., Ahmaruzzaman, M., Adhikari, P. P. & Bora, R. T. Green and environmentally sustainable fabrication of Ag-SnO2 Nanocomposite and its multifunctional efficacy as photocatalyst and antibacterial and antioxidant Agent. *ACS Sustainable Chem. Eng.* **5** (6), 4645–4655 (2017).

18. Mou, H., Song, C., Zhou, Y., Zhang, B. & Wang, D. Design and synthesis of porous Ag/ZnO nanosheets assemblies as super photocatalysts for enhanced visiblelight degradation of 4-nitrophenol and hydrogen evolution. *Appl. Catal. B.* **221**, 565–573 (2018).
19. Teixeira, L. B., Fernandes, V. K., Maia, B. G. O., Arcaro, S. & Novaes de Oliveira, A. P. Vitrocrystalline foams produced from glass and oyster shell wastes. *Ceram. Int.* **43** (9), 6730–6737 (2017).
20. Sawai, J. Quantitative evaluation of antibacterial activities of metallic oxide powders (ZnO, MgO and CaO) by conductimetric assay. *J. Microbiol. Methods*. **54** (2), 177–182 (2003).
21. Lipovsky, A., Nitzan, Y., Gedanken, A. & Lubart, R. Antifungal activity of ZnO nanoparticles—the role of ROS mediated cell injury. *Nanotechnology* **22**, 105101 (2011).
22. Chang, L. et al. Dual functional oyster shell-derived Ag/ZnO/$CaCO_3$ nanocomposites with enhanced catalytic and antibacterial activities for water purification. *RSC Adv.* **9**, 41336–41344 (2019).
23. Huang, X. et al. Plant-mediated synthesis of dual-functional Eggshell/Ag nanocomposites towards catalysis and antibacterial applications. *Mater. Sci. Eng. C.* **113**, 1110152 (2020).
24. Almohefer, S. A., Levon, J. A., Gregory, R. L., Eckert, G. J. & Lippert, F. Caries lesion remineralization with fluoride toothpastes and chlorhexidine - effects of application timing and toothpaste surfactant. *J. Appl. oral Sci.* **26**, e20170499 (2018).
25. Kim, Y. M. et al. Antibacterial and remineralization effects of orthodontic bonding agents containing bioactive glass. *Korean J. Orthod.* **48** (3), 163–171 (2018).
26. Huang, X. et al. Application Study of Novel Eggshell/Ag combined with pit and fissure sealants. *Int. J. Nanomed.* **18**, 2911–2922 (2023).
27. Tao, S. et al. Nano-calcium phosphate and dimethylaminohexadecyl methacrylate adhesive for dentin remineralization in a biofilm-challenged environment. *Dent. Mater.* **36** (10), e316–e328 (2020).
28. Fan, M. et al. Remineralization effectiveness of the PAMAM dendrimer with different terminal groups on artificial initial enamel caries in vitro. *Dent. Mater.* **36** (2), 210–220 (2020).
29. Tenuta, L. M. & Cury, J. A. Laboratory and human studies to estimate anticaries efficacy of fluoride toothpastes. *Monogr. Oral Sci.* **23**, 108–124 (2013).
30. Ruan, Q. et al. Efficacy of amelogenin-chitosan hydrogel in biomimetic repair of human enamel in pH-cycling systems. *J. Biomedical Eng. Inf.* **2** (1), 119–128 (2016).
31. Lippert, F. & Juthani, K. Fluoride dose-response of human and bovine enamel artificial caries lesions under pH-cycling conditions. *Clin. Oral Invest.* **19** (8), 1947–1954 (2015).
32. Hannas, A. R. et al. Preventive effect of toothpastes with MMP inhibitors on human dentine erosion and abrasion in vitro. *J. Appl. Oral Sci.* **24** (1), 61–66 (2016).
33. Wang, X. et al. Bifunctional anticaries peptides with antibacterial and remineralizing effects. *Oral Dis.* **25** (2), 488–496 (2019).
34. Fontana, M. et al. Measurement of enamel demineralization using microradiography and confocal microscopy. A correlation study. *Caries Res.* **30** (5), 317–325 (1996).
35. State Food and Drug Administration. *YY/T 0127.13. Biological Evaluation of Oral Medical Devices Unit 2: Test Methods-Oral Mucosal Irritation Test (Chinese)* (China Standard, 2010).
36. Lv, X. et al. Potential of an amelogenin based peptide in promoting reminerlization of initial enamel caries. *Arch. Oral Biol.* **60** (10), 1482–1487 (2015).
37. Armentano, I. et al. The interaction of bacteria with engineered nanostructured polymeric materials: a review. The Scientific World Journal. ; 2014: 410423. (2014).
38. Li, H., Chen, Q., Zhao, J. & Urmila, K. Enhancing the antimicrobial activity of natural extraction using the synthetic ultrasmall metal nanoparticles. *Sci. Rep.* **5**, 11033 (2015).
39. Luan, B., Huynh, T. & Zhou, R. Complete wetting of graphene by biological lipids. *Nanoscale* **8** (10), 5750–5754 (2016).
40. Gao, W., Thamphiwatana, S., Angsantikul, P. & Zhang, L. Nanoparticle approaches against bacterial infections. *Wiley Interdisciplinary Reviews Nanomed. Nanobiotechnol.* **6** (6), 532–547 (2014).
41. Gurunathan, S., Han, J. W., Dayem, A. A., Eppakayala, V. & Kim, J. H. Oxidative stress-mediated antibacterial activity of graphene oxide and reduced graphene oxide in Pseudomonas aeruginosa. *Int. J. Nanomed.* **7**, 5901–5914 (2012).
42. Zakharova, O. V. et al. Considerable Variation of Antibacterial Activity of Cu Nanoparticles Suspensions Depending on the Storage Time, Dispersive Medium, and Particle Sizes. BioMed research international. ; 2015: 412530. (2015).
43. Yang, W. et al. Food storage material silver nanoparticles interfere with DNA replication fidelity and bind with DNA. *Nanotechnology* **20** (8), 085102 (2009).
44. Wang, L., Hu, C. & Shao, L. The antimicrobial activity of nanoparticles: present situation and prospects for the future. *Int. J. Nanomed.* **12**, 1227–1249 (2017).
45. Wang, Z., Jiang, S., Zhao, Y. & Zeng, M. Synthesis and characterization of hydroxyapatite nano-rods from oyster shell with exogenous surfactants. *Mater. Sci. Eng., C.* **105**, 110102 (2019).
46. Panacek, A. et al. Silver colloid nanoparticles: synthesis, characterization, and their antibacterial activity. *J. Phys. Chem. C.* **110** (33), 16248–16253 (2006).
47. Qasim, M., Udomluck, N., Chang, J., Park, H. & Kim, K. Antimicrobial activity of silver nanoparticles encapsulated in poly-N-isopropylacrylamide-based polymeric nanoparticles. *Int. J. Nanomed.* **13**, 235–249 (2018).
48. Morones, J. R. et al. The bactericidal effect of silver nanoparticles. *Nanotechnology* **16** (10), 2346–2353 (2005).
49. Li, J. et al. Highly selective antibacterial activities of silver nanoparticles against Bacillus subtilis. *J. Nanosci. Nanotechnol.* **13** (10), 6806–6813 (2013).
50. Lipovsky, A., Nitzan, Y., Gedanken, A. & Lubart, R. Antifungal activity of ZnO nanoparticles–the role of ROS mediated cell injury. *Nanotechnology* **22** (10), 105101 (2011).
51. Tian, X. et al. *ACS Appl. Mater. Interfaces* ; **10**: 8443–8450. (2018).
52. Katsikogianni, M. & Missirlis, Y. F. Concise review of mechanisms of bacterial adhesion to biomaterials and of techniques used in estimating bacteria-material interactions. *Eur. Cells Mater.* **8**, 37–57 (2004).
53. Scheie, A. A. & Petersen, F. C. The Biofilm Concept: consequences for future prophylaxis of oral diseases? *Crit. Reviews Oral Biology Med.* **15** (1), 4–12 (2004).
54. Ulagesan, S., Krishnan, S., Nam, T. J. & Choi, Y. H. A review of Bioactive compounds in Oyster Shell and tissues. *Front. Bioeng. Biotechnol.* **10**, 913839 (2022).
55. Churchley, D. et al. Protection against enamel demineralisation using toothpastes containing o-cymen-5-ol, zinc chloride and sodium fluoride. *Int. Dent. J.* **61** (Suppl 3), 55–59 (2011).
56. Mohammed, N. R. et al. Physical chemical effects of zinc on in vitro enamel demineralization. *J. Dent.* **42** (9), 1096–1104 (2014).
57. Rahman, M. T., Hossain, A., Pin, C. H. & Yahya, N. A. Zinc and Metallothionein in the Development and Progression of Dental Caries. *Biol. Trace Elem. Res.* **187** (1), 51–58 (2019).

Acknowledgements
Not applicable.

Author contributions

Chang conducted the study and wrote the main manuscript; Gan and Huang reviewed and revised the manuscript; Su collected and processed the data; Zheng led the planning of the research activities; Feng and Lu managed and coordinated the execution of the research activities. All authors reviewed the manuscript.

Funding

The research project was supported by Natural Sciences Foundation of Fujian Province (grant number 2021J01801 and 2022J01767);Finance Department of Fujian Province (grant number 2021CZ01); the Open Project of Fujian Provincial Engineering Research Center of Oral Biomaterial (grant number 2021KQ01).

Declarations

Ethics approval and consent to participate

All methods were carried out in accordance with relevant guidelines and regulations.

Consent for publication

All listed authors consent to the submission.

Competing interests

The authors declare no competing interests.
All methods are reported in accordance with ARRIVE guidelines (https://arriveguidelines.org).

Additional information

Correspondence and requests for materials should be addressed to Y.L. or Y.F.

Reprints and permissions information is available at www.nature.com/reprints.

Publisher's note Springer Nature remains neutral with regard to jurisdictional claims in published maps and institutional affiliations.